Article

A Fast Surrogate Model-Based Algorithm Using Multilayer Perceptron Neural Networks for Microwave Circuit Design

Mohammad (Behdad) Jamshidi [1], Salah I. Yahya [2,3], Saeed Roshani [4], Muhammad Akmal Chaudhary [5], Yazeed Yasin Ghadi [6] and Sobhan Roshani [4,*]

[1] The International Association of Engineers (IAENG), Hong Kong 999077, China
[2] Department of Communication and Computer Engineering, Cihan University-Erbil, Erbil 44001, Iraq
[3] Department of Software Engineering, Faculty of Engineering, Koya University, Koya 46017, Iraq
[4] Department of Electrical Engineering, Kermanshah Branch, Islamic Azad University, Kermanshah 67771, Iran
[5] Department of Electrical and Computer Engineering, College of Engineering and Information Technology, Ajman University, Ajman P.O. Box 346, United Arab Emirates
[6] Software Engineering and Computer Science Department, Al Ain University, Al Ain P.O. Box 15551, United Arab Emirates
[*] Correspondence: s.roshani@aut.ac.ir or sobhan_roshany@yahoo.ca

Abstract: This paper introduces a novel algorithm for designing a low-pass filter (LPF) and a microstrip Wilkinson power divider (WPD) using a neural network surrogate model. The proposed algorithm is applicable to various microwave devices, enhancing their performance and frequency response. Desirable output parameters can be achieved for the designed LPF and WPD by using the proposed algorithm. The proposed artificial neural network (ANN) surrogate model is employed to calculate the dimensions of the LPF and WPD, resulting in their efficient design. The LPF and WPD designs incorporate open stubs, stepped impedances, triangular-shaped resonators, and meandered lines to achieve optimal performance. The compact LPF occupies a size of only $0.15 \lambda g \times 0.081 \lambda g$, and exhibits a sharp response within the transmission band, with a sharpness parameter of approximately 185 dB/GHz. The designed WPD, operating at 1.5 GHz, exhibits outstanding harmonics suppression from 2 GHz to 20 GHz, with attenuation levels exceeding 20 dB. The WPD successfully suppresses 12 unwanted harmonics (2nd to 13th). The obtained results demonstrate that the proposed design algorithm effectively accomplishes the LPF and WPD designs, exhibiting desirable parameters such as operating frequency and high-frequency harmonics suppression. The WPD demonstrates a low insertion loss of 0.1 dB (S_{21} = 0.1 dB), input and output return losses exceeding 30 dB (S_{11} = −35 dB, S_{22} = −30 dB), and an output ports isolation of more than 32 dB (S_{23} = −32 dB), making it suitable for integration into modern communication systems.

Keywords: design algorithm; low-pass filter; power divider; neural network

1. Introduction

Recently, artificial intelligence (AI) and artificial neural network (ANN) models have been widely utilized to solve engineering problems [1,2]. Machine learning approaches have emerged as powerful tools for addressing nonlinear problems and gaining valuable insights from complex systems [3,4]. These approaches harness the computational capabilities of artificial neural networks, such as multilayer perceptron architectures, to capture and analyze the nonlinear dynamics inherent in these systems. By training neural networks on data obtained from complex systems, researchers have successfully captured their underlying behaviors, enabling precise predictions and enhanced control of these systems [5].

In particular, ANNs have been used to ease the design and improve the performance of electronics devices, such as microwave devices [6–8]. Filters and power dividers are vital blocks in new microwave and communications circuits [9]. In modern microwave circuits, a compact size and harmonics rejection are required to reduce the circuit area and costs [10].

Additionally, rejection of harmonics results in the improvement of the the given system's overall performance [11]. The conventional power dividers previously used in microwave circuits occupy a large area, and cannot reject undesirable harmonics. Therefore, recently, different designs have been introduced to overcome these drawbacks. Previous research aiming to counteract the disadvantages of conventional power dividers are explained in the following section. Nonlinear phenomena present significant challenges when it comes to comprehending and predicting the behavior of complex systems. This holds true in various engineering fields, including microwave circuit design, medical engineering, industrial engineering, etc., wherein accurate modeling and analysis play a vital role in optimizing performance and ensuring reliability [12–15]. However, traditional analytical approaches often struggle to capture the intricate dynamics exhibited by nonlinear systems, prompting the exploration of alternative methods [16].

EBG and DGS techniques have been used in [17–19] to decrease the circuit size and suppress undesirable harmonies. However, these methods require extra steps in the device implementation process, which is undesirable. In some works [20–22], open stubs have been used for harmonics suppression and size reduction purposes. However, only a few harmonics can be suppressed using open stubs, and a significant reduction in size cannot be obtained. A WPD with two main open stubs and three coupled lines is designed in [20], in which a wide band and filtering response with high attenuation was obtained. In [21], triangular-shaped open stubs are incorporated in the device's structure in order to present a coupler with rejection band, which achieved a bandwidth of 200 MHz within a main frequency of 700 MHz. A coupler with rectangular open stubs is designed in [22], and achieved filtering response and harmonic rejection.

In many designs [23–31], resonators and filters have been used in the divider structure to suppress harmonics. Applied resonators increase the complexity of circuits, and if resonators are not used properly, they may also increase insertion loss. In [23], a WPD with rectangular stubs and coupled line resonators is presented. The applied resonators in [23] reduced the overall size of the designed WPD. A multi-mode resonator and coupling lines are incorporated int the presented WPD in [25] to achieve a small size and high selectivity. A coupled line, T-shaped resonators, and open stubs are exploited in [26] within the design of a divider; this achieved dual band operation and a filtering response. The presented work in [27] proposes a miniaturized WPD that uses rectangular resonator cells instead of quarter-wave length branches, which reduced the circuit size, increased the bandwidth, and eliminated unwanted harmonics. The WPD presented in [28] uses complementary split-ring resonators (CSRRs) for harmonic suppression. The work presented in [29] proposes a dual-band filtering power divider that employs dual-resonance resonators (DRRs) to create multiple transmission zeros, resulting in two passbands with high-frequency selectivity, good isolation, and an ultra-wide stopband. A tri-band WPD is designed in [30], using resonators that replace each quarter-wavelength transformer in the conventional WPD. Additionally, the WPD presented in [31] uses quasi-elliptic filters to replace each quarter-wavelength transformer for improved out-of-band rejection.

Moreover, due to the higher frequency limitations of Microstrip substrates, crystal photonics have been widely applied in high-frequency designs [32–35]. This method [36,37] can be used for passive design structures, such as power dividers, in higher frequency ranges. Additionally, in some designs [38–43], lumped components (L and C) have been used to create compact dividers with harmonics suppression that then cause a limited frequency response. The work presented in [40] discusses the design and implementation of a five-way lumped-element WPD to investigate multifrequency polarimetric SAR applications. the use of flexible and miniaturized lumped elements in the design of unequal Wilkinson power dividers is studied in [41], utilizing closed-form design methods for frequency characteristics' simulation. A lumped-element WPD using LC-ladder circuits composed of a capacitor and an inductor, alongside a series LR/CR circuit, is designed in [42]; this theoretically shows that broadband WPDs can be accomplished. Additionally,

in [43], a compact structure for a dual-band WPD is proposed; it consists of a single line, two coupled lines, and four lumped elements.

Overall, these designs demonstrate the effectiveness of using several techniques, such as incorporating resonators, open stubs, and lumped components, in the design of WPD and couplers to achieve desirable circuit performance in modern communication systems. However, in all of the mentioned approaches, there is no straightforward algorithm to ease the design procedures of the device's structure using desirable parameters; this task is very complicated. In this paper, a new design algorithm is presented to help in the design of complicated devices in microwave and communication systems, such as filters and power dividers, with easy steps. In this paper, two filters and a single open stub are used together to shape the proposed divider at 1.5 GHz, using the proposed design algorithm. With this algorithm, more than 12 unwanted harmonics (2nd–13th) are suppressed, and a wide suppression band from 2 GHz to 20 GHz is provided.

2. Design Algorithm

The application of machine learning techniques, particularly neural networks, has shown considerable promise across various domains. For example, in structural engineering, machine learning algorithms have been employed to analyze and predict the behavior of complex structures subjected to different loads and environmental conditions. By leveraging extensive datasets and learning patterns, these algorithms facilitate accurate predictions of structural responses, fatigue life, and failure modes. In the realm of microwave circuit design, the complexities associated with nonlinear phenomena and intricate engineering issues necessitate the development of efficient and accurate modeling techniques. This paper aims to introduce a fast surrogate model-based algorithm that utilizes multilayer perceptron neural networks specifically for microwave circuit design. By incorporating machine learning techniques, this algorithm seeks to address the design challenges in microwave circuits and provide valuable insights for design optimization [44,45].

In this section, as shown in Figure 1, the proposed design algorithm is presented to help to design complicated devices within microwave and communication systems, particularly, filters and power dividers. In Step 1 of the proposed design algorithm, the preliminary LPF is presented, in which the dimensions are not finalized. The presented LPF may have any arbitrary structure. In Step 2, the ANN structure is proposed for the presented LPF. Then, the proposed ANN model is trained using an electromagnetic simulation of the preliminary resonator in Step 3. The dimensions of the preliminary LPF may be finalized by the ANN, based on the LPF desired parameters and the predicted data, as shown in Step 4; the final LPF can be created in Step 5. After applying the proposed final LPFs to the two main branches of the divider (Step 6), the final WPD may be achieved, as detailed in Step 7.
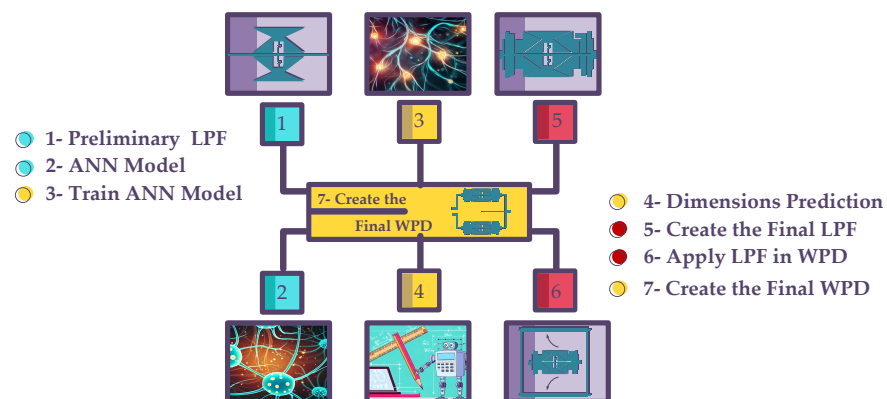

1- Preliminary LPF
2- ANN Model
3- Train ANN Model
4- Dimensions Prediction
5- Create the Final LPF
6- Apply LPF in WPD
7- Create the Final WPD

Figure 1. The presented design algorithm used to design the proposed power divider, which is described in seven steps.

2.1. The Architecture of the Proposed ANN Model

The proposed model includes a multi-layer feed forward network neural network (ANN), which can predict the desired output parameters by considering the circuit parameters. The proposed model works as a surrogate model to predict the parameters of the proposed filter. Figure 2 shows the proposed MLP structure for the defined artificial network. According to this figure, the input parameter is connected to output nodes by two hidden layers, including seven neurons in each hidden layer. Additionally, the values of fc (GHZ), ζ (dB/GHz), BW (MHZ), and RL (dB), which are desirable resonator parameters, are considered the output of the proposed ANN model.
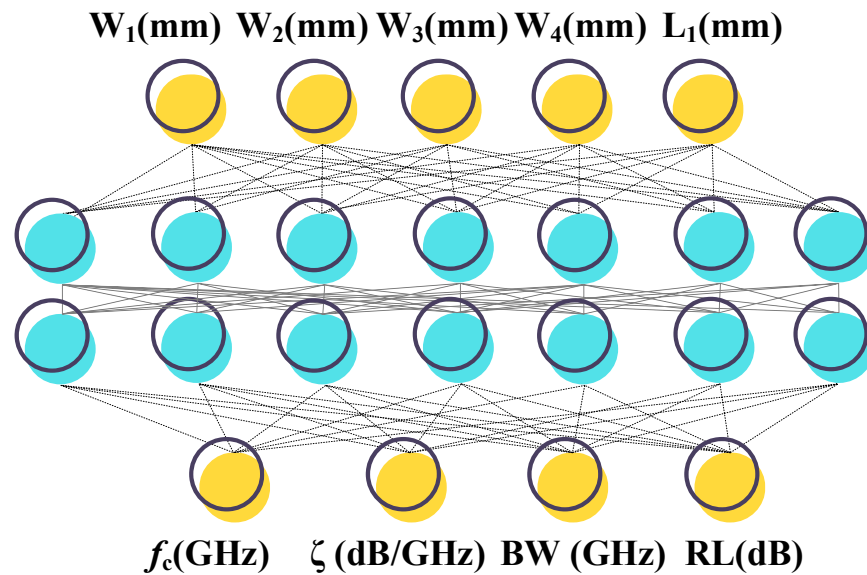
$$W_1(mm) \quad W_2(mm) \quad W_3(mm) \quad W_4(mm) \quad L_1(mm)$$

$$f_c(GHz) \quad \zeta\ (dB/GHz) \quad BW\ (GHz) \quad RL(dB)$$

Figure 2. Proposed structure of the ANN model, including two hidden layers with seven neurons in each hidden layer.

A flowchart of the proposed structure of the ANN is illustrated in Figure 3. As shown, within the first step, the structure of the network, the hidden layer numbers, and the neuron numbers are considered, due to the input and output parameters and the problem conditions. In the next steps, the weights and biases of the ANN are defined randomly; then, as explained in the flow chart, these values are calculated using the proposed ANN model. Finally, after reaching the desired accuracy, the ANN model is created.
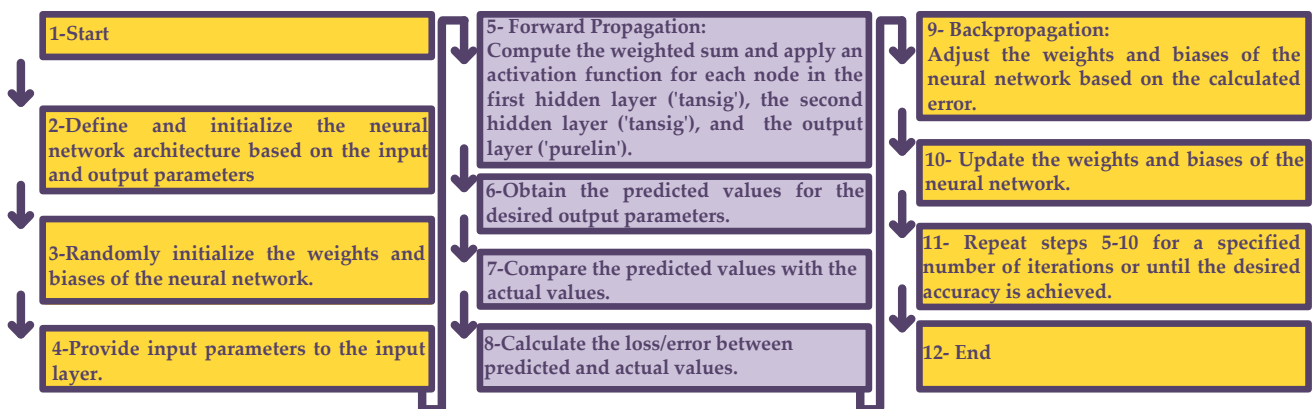

1-Start

2-Define and initialize the neural network architecture based on the input and output parameters

3-Randomly initialize the weights and biases of the neural network.

4-Provide input parameters to the input layer.

5- Forward Propagation: Compute the weighted sum and apply an activation function for each node in the first hidden layer ('tansig'), the second hidden layer ('tansig'), and the output layer ('purelin').

6-Obtain the predicted values for the desired output parameters.

7-Compare the predicted values with the actual values.

8-Calculate the loss/error between predicted and actual values.

9- Backpropagation: Adjust the weights and biases of the neural network based on the calculated error.

10- Update the weights and biases of the neural network.

11- Repeat steps 5-10 for a specified number of iterations or until the desired accuracy is achieved.

12- End

Figure 3. The flowchart of the proposed structure of the ANN.

In a multi-layer feed-forward neural network, the values of neurons in the hidden layers are updated through a process called forward propagation and backpropagation. The first step is initialization, in which the weights and biases of the neural network are

randomly initialized. The next step is forward propagation, in which input values are provided to the input layer, the weighted sum of inputs for each neuron in the first hidden layer is computed, and an activation function is applied to the computed sum, producing an output value for each neuron in the first hidden layer. The same process is repeated for the second hidden layer, using the output values from the first hidden layer as inputs. Then, the weighted sum of inputs for each neuron in the output layer is computed, and an activation function is applied to the computed sum, thus generating the final output values of the neural network [46,47]. In the proposed ANN model, the hyperbolic tangent activation function ('tansig') is used for the first and the second hidden layers, while the linear activation function ('purelin') is used for the output layer.

The next step is backpropagation, in which the error between the predicted output values and the actual output values is calculated; then, the weights and biases in the output layer are updated using the calculated error and an optimization algorithm. The next step is backpropagating the error to the second hidden layer; then, the error contribution of each neuron in the second hidden layer is calculated, based on the weights connecting it to the output layer and the propagated error from the output layer. In the next level, the weights and biases are updated in the second hidden layer, using the calculated error contribution and the optimization algorithm. By repeating the same process for the first hidden layer, the error from the second hidden layer is backpropagated, and the corresponding weights and biases are updated [47,48].

Then, the forward propagation and backpropagation steps are repeated for each training sample in the training set. Additionally, the weights and biases are adjusted iteratively, based on the error calculated for each sample. During training, the weights and biases are updated gradually, allowing the neural network to learn the underlying patterns and to optimize its predictions. By iteratively updating the weights and biases through forward propagation and backpropagation, the neural network adjusts its internal parameters to minimize the error between the predicted and actual output values, ultimately improving its ability to make accurate predictions [49].

2.2. Proposed Resonator Design

In order to achieve the desired performance and features, such as small dimensions, a wide stop-band bandwidth, and a sharp response in the transient region of the resonator, within the first step, a preliminary resonator should be designed. First, a simple compact resonator is proposed (regarding the desired frequency), and then the results are improved by adding another resonators and suppressors. It should be noted that all of the simulations were carried out using ADS software.

2.3. Proposed Basic Single Polygonal Resonator Design

The structure of the basic single polygonal resonator with a folded transmission line is demonstrated in Figure 4. The proposed resonators were designed on an RT/Duroid 5880 substrate with a dielectric coefficient of 2.2 and a dielectric thickness of 0.508 mm. This resonator has a transition zero at a frequency of 2.75 GHz.
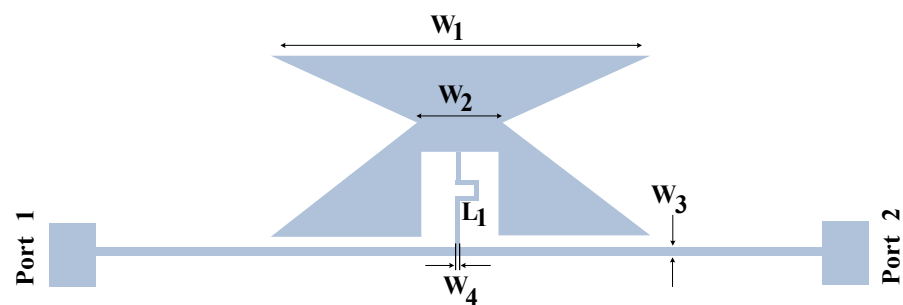

Figure 4. The structure of the proposed basic single polygonal resonator, loaded with a folded transmission line.

2.4. Proposed Preliminary Dual Polygonal Resonator Design

In order to improve the results, a preliminary dual polygonal resonator with a symmetrical structure is proposed, as seen in Figure 5.
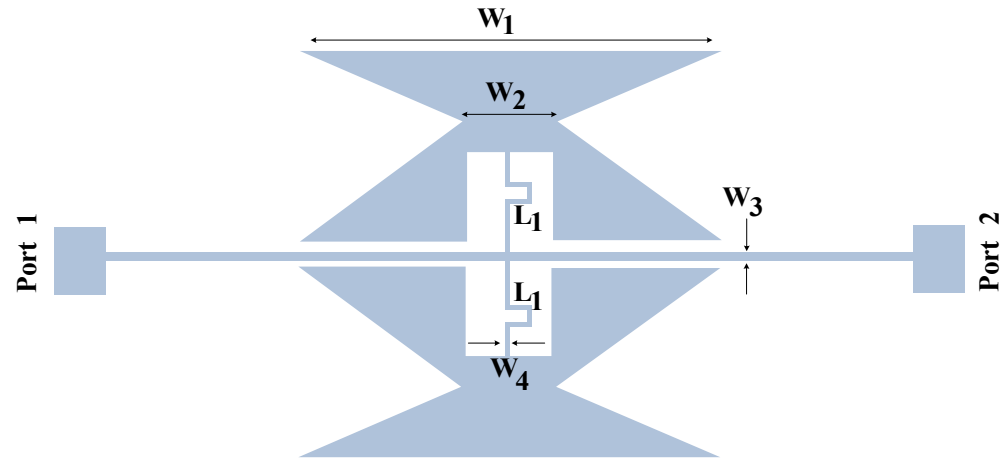

Figure 5. The structure of the proposed preliminary dual polygonal resonator, loaded with folded transmission lines.

2.5. Applying The Proposed ANN Model

In the presented ANN model, 31 samples are used for training of the network, while 7 and 2 samples are used for the testing and validation of the proposed surrogate model, respectively. In the proposed ANN, the mean relative error (*MRE*) and root mean square error (*RMSE*) are considered in order to evaluate the proposed model results as follows.

$$MRE = \frac{1}{N}\sum_{i=1}^{N}\left|\frac{Y_{Ri} - Y_{Pi}}{Y_{Ri}}\right|. \tag{1}$$

$$RMSE = \sqrt{\frac{\sum_{i=1}^{N}(Y_{Ri} - Y_{Pi})^2}{N}}. \tag{2}$$

where N is total number of the dataset, and Y_{Ri} and Y_{Pi} are the real and predicted output of the presented ANNs, respectively.

3. The Results of the Proposed ANN Model

As mentioned, the presented model structure with two hidden layers and seven neurons in each hidden layer is selected as the most precise model. The real and predicted comparison values of the f_c (GHZ), ζ (dB/GHz), BW (MHZ), and RL (dB) parameters for the training and testing data are shown in Figure 6. As shown, the circuit parameters are predicted with acceptable accuracy. According to in Figure 6, the test errors are higher compared to the training errors, but the values of error are acceptable, and the worst-case error for both the testing and the training process is below than 0.2 MRE. In addition, the obtained results of the proposed filter and power divider, predicted using the proposed ANN, show that the small difference between the real and predicted data in the testing process did not affect the filter and power divider output parameters, and the desired results were obtained for the designed filter and divider.
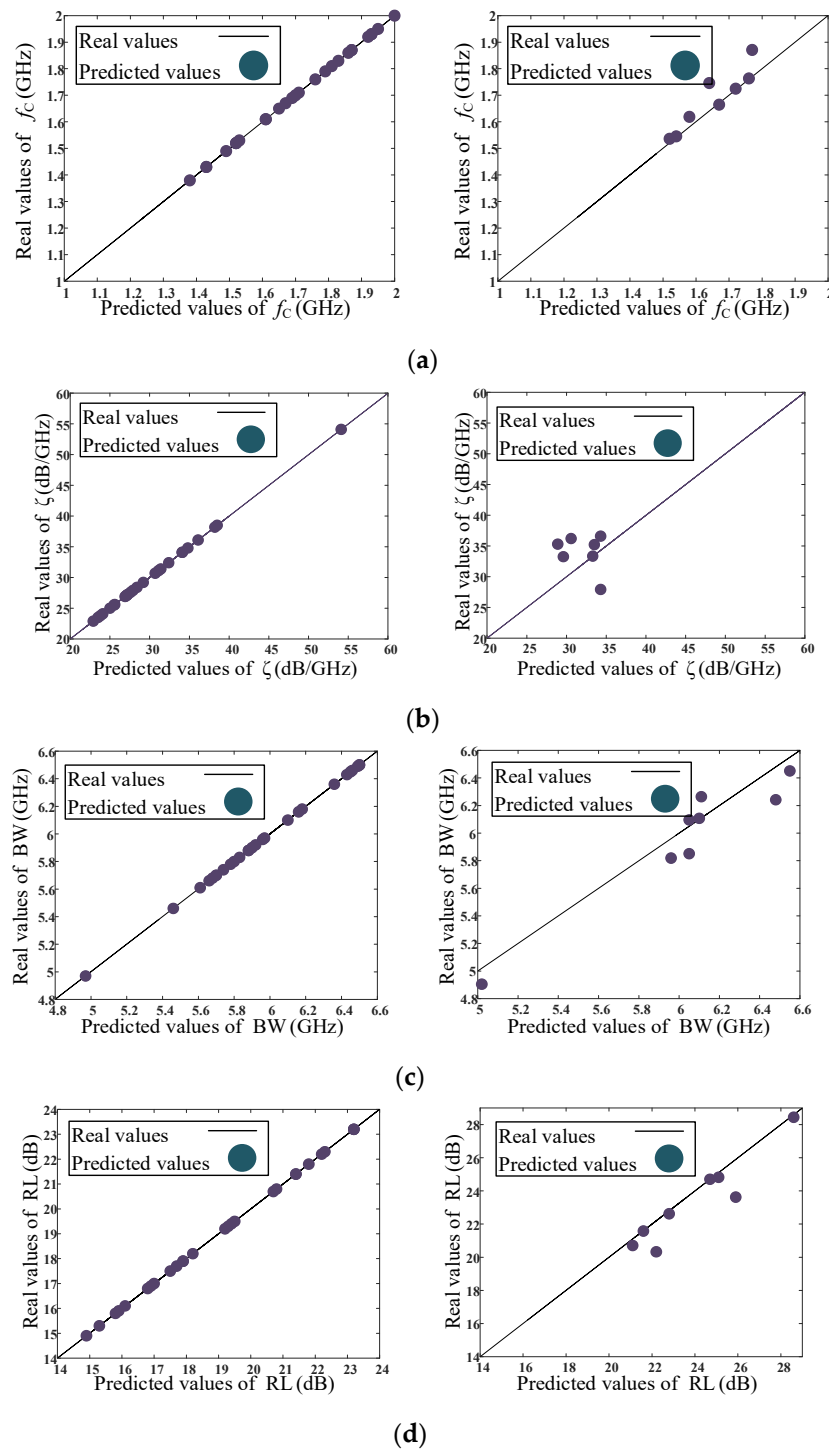
Figure 6. The real and predicted comparison values for the training and testing data, using the proposed model. Real and predicted values of (**a**) f_c (GHZ), (**b**) ζ (dB/GHz), (**c**) BW (MH), and (**d**) RL (dB).

The real and predicted testing and training values of the f_c (GHZ), ζ (dB/GHz), BW (MHZ), and RL (dB) parameters versus the number of data samples in the proposed model are shown in Figure 7. As seen, the circuit parameters were predicted with acceptable accuracy. Two samples were chosen for validation, and these are shown in Figure 7. The validation samples validate the accuracy of the proposed model, and help in designing the proposed resonator with the desired parameters.
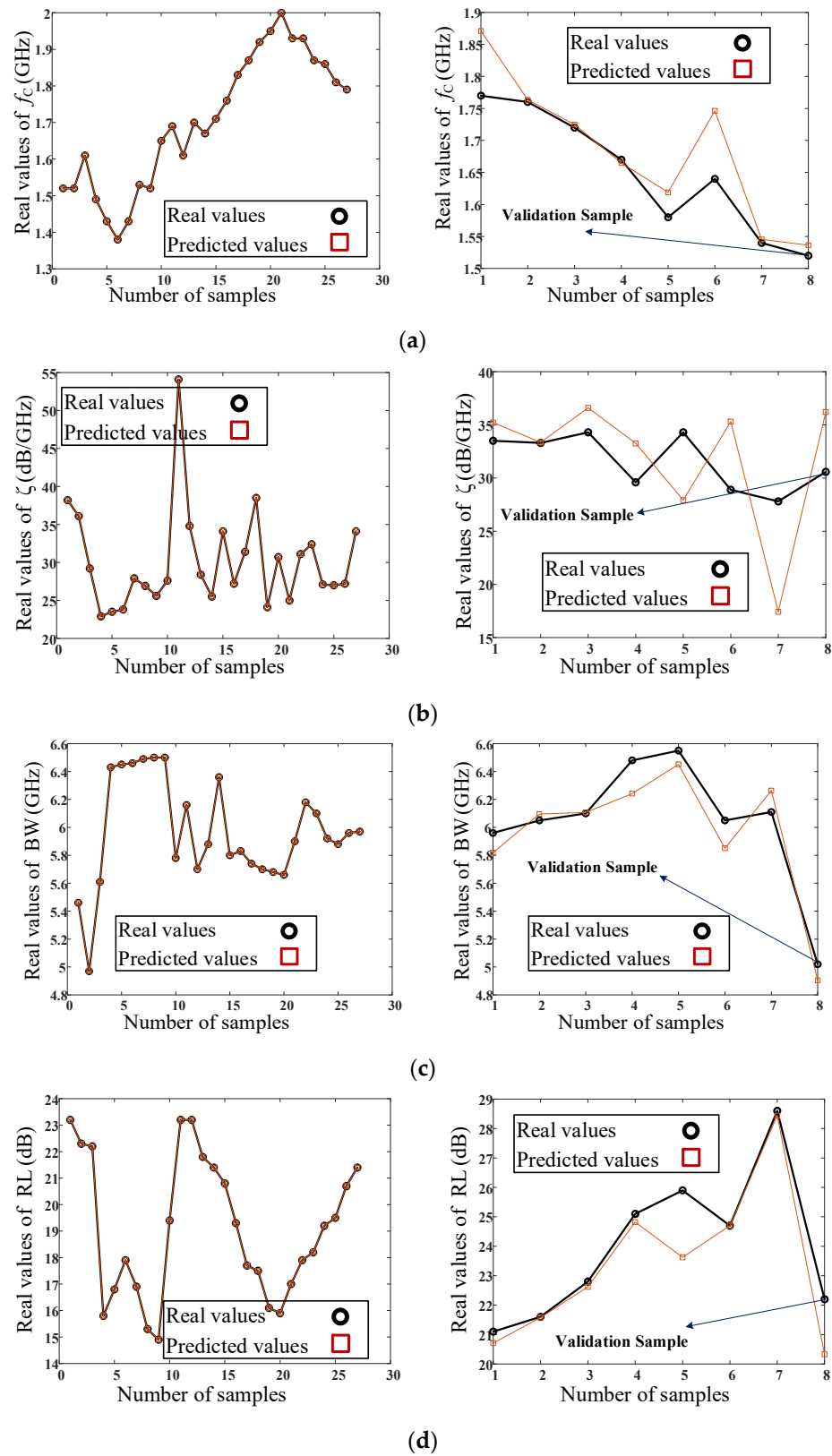
Figure 7. Real and predicted testing and training values of (**a**) f_c (GHZ), (**b**) ζ (dB/GHz), (**c**) BW (MHZ), and (**d**) RL (dB) parameters versus number of data samples in the proposed model. The left plots correspond to the training process, and the right plots correspond to the testing and verification processes of the proposed model.

The real data of the training, testing, and validation procedures, using the proposed model are listed in Table 1. As seen, 27 samples are considered for training, 7 samples are considered for testing, and 1 sample is taken into account for the validation of the proposed ANN surrogate model.

Table 1. The real data of the training, testing, and validation procedures, using the proposed model.

	W_1 (mm)	W_2 (mm)	W_3 (mm)	W_4 (mm)	L_1 (mm)	f_o (GHz)	ζ (dB/GHz)	BW (MHz)	RL (dB)
					Training Values				
			Input Parameters				Output Parameters		
1	10.7	2.2	0.2	0.1	18.7	1.52	38.2	5.46	23.2
2	10.7	1	0.2	0.1	18.7	1.52	36.1	4.97	22.3
3	10.7	1	0.2	0.2	18.7	1.61	29.2	5.61	22.2
4	10.7	1	0.1	0.2	18.7	1.49	22.9	6.43	15.8
5	11.3	1	0.1	0.2	18.7	1.43	23.5	6.45	16.8
6	11.3	2	0.1	0.2	18.7	1.38	23.8	6.46	17.9
7	10.7	2	0.1	0.2	18.7	1.43	27.9	6.49	16.9
8	10	2	0.1	0.2	18.7	1.53	26.9	6.5	15.3
9	10	1.6	0.1	0.2	18.7	1.52	25.6	6.5	14.9
10	10	1.6	0.2	0.2	18.7	1.65	27.6	5.78	19.4
11	10	1.6	0.2	0.2	16.3	1.69	54.1	6.16	23.2
12	10	1.6	0.2	0.1	16.3	1.61	34.8	5.7	23.2
13	9.5	1.6	0.2	0.1	16.3	1.7	28.4	5.88	21.8
14	9.5	1.4	0.2	0.1	16.3	1.67	25.5	6.36	21.4
15	9.5	1	0.2	0.1	16.3	1.71	34.1	5.8	20.8
16	8.9	1	0.2	0.1	16.3	1.76	27.2	5.83	19.3
17	8.3	1	0.2	0.1	16.3	1.83	31.4	5.74	17.7
18	8.3	0.8	0.2	0.1	16.3	1.87	38.5	5.7	17.5
19	7.7	0.8	0.2	0.1	16.3	1.92	24.1	5.68	16.1
20	7.7	0.6	0.2	0.1	16.3	1.95	30.7	5.66	15.9
21	7.7	0.6	0.2	0.1	15.3	2	25	5.9	17
22	8.2	0.6	0.2	0.1	15.3	1.93	31.1	6.18	17.9
23	8.2	0.8	0.2	0.1	15.3	1.93	32.4	6.1	18.2
24	8.5	0.8	0.2	0.1	15.3	1.87	27.1	5.92	19.2
25	8.5	1	0.2	0.1	15.3	1.86	27	5.88	19.5
26	8.9	1	0.2	0.1	15.3	1.81	27.2	5.96	20.7
27	9.2	1	0.2	0.1	15.3	1.79	34.1	5.97	21.4
					Testing Values				
			Input Parameters				Output Parameters		
1	9.2	0.6	0.2	0.1	15.3	1.77	33.5	5.96	21.1
2	9.2	1.1	0.2	0.1	15.3	1.76	33.3	6.05	21.6
3	9.6	1.1	0.2	0.1	15.3	1.72	34.3	6.1	22.8
4	10.1	1.1	0.2	0.1	15.3	1.67	29.6	6.48	25.1
5	10.1	1.5	0.2	0.1	15.3	1.58	34.3	6.55	25.9
6	10.1	0.9	0.2	0.1	15.3	1.64	28.9	6.05	24.7
7	11.1	0.9	0.2	0.1	15.3	1.54	27.8	6.11	28.6
					Validation Values				
			Input Parameters				Output Parameters		
1	9.9	2.2	0.2	0.1	18.7	1.52	30.58	5.02	22.2

The final results of the proposed ANN model are listed in Table 2, which shows the high accuracy of the predictions of the proposed model. The errors reported in this table correspond to the denormalized data. According to this table, the model was trained perfectly using the training data. Additionally, the validation sample was accurately

predicted by the proposed model, which was then used to form the structure of the proposed resonator.

Table 2. The final results of the proposed ANN model.

	f_o (GHz) Errors			ζ (dB/GHz) Errors			BW (MHz) Errors			RL (dB) Errors		
	Training	Testing	Valid.	Training	Testing	Valid.	Training	Testing	Valid.	Training	Testing	Valid.
MRE	2.97×10^{-7}	0.0226	0.0163	3.99×10^{-7}	0.1464	0.1841	9.87×10^{-10}	0.0203	0.0230	6.30×10^{-10}	0.0188	0.0844
RMSE	3.01×10^{-6}	0.0574	0.0163	1.09×10^{-4}	5.4911	5.6301	9.01×10^{-9}	0.1474	0.1157	2.07×10^{-8}	0.8833	1.8727

4. The Design of the Proposed Filter

After predicting the dimension values of the proposed preliminary dual polygonal resonator from the validation sample of the proposed ANN model, its frequency response is shown in Figure 8. As can be seen from the frequency response, this resonator has a transition zero with more than a 60 dB attenuation level. Additionally, the dual polygonal resonator has an insertion loss of about 0.5 dB in the pass band. The dimensions of the proposed preliminary dual polygonal resonator, predicted by the ANN, are listed as follows: $L_1 = 1.2$ mm, $W_1 = 1.56$ mm, $L_7 = 0.8$ mm, $W_7 = 9.9$ mm, $L_8 = 0.8$ mm, $W_8 = 2.2$ mm, $W_9 = 0.1$ mm, $W_{10} = 0.2$ mm, $S = 0.2$ mm, $L_T = 19.3$ mm, $W_T = 9.9$ mm.
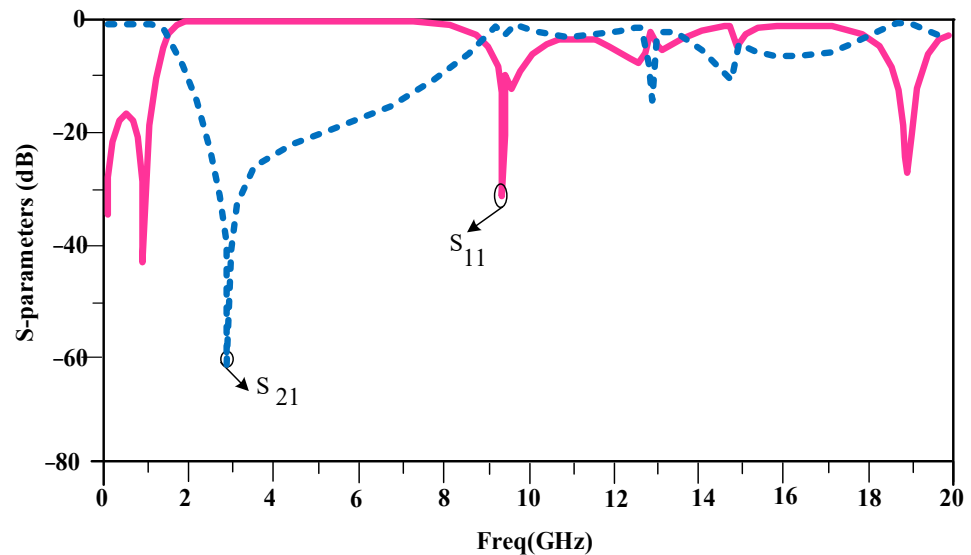
Figure 8. The S-parameter results of the proposed dual polygonal resonator, loaded with folded transmission lines.

4.1. The Design of the Proposed Dual Side Resonators

In order to improve the results and to obtain a microstrip low-pass filter with smaller dimensions, two dual-side resonators were designed and loaded at the main transmission line of the filter. The structure of these resonators is depicted in Figure 9. The dimensions of the proposed dual-side resonators, which are depicted in Figure 9, are listed as follows: $L_1 = 1.2$ mm, $W_1 = 1.56$ mm, $L_5 = 3$ mm, $W_5 = 0.1$ mm, $L_6 = 1.8$ mm, $W_6 = 1.4$ mm, $L_7 = 0.8$ mm, $W_7 = 9.9$ mm, $L_8 = 0.8$ mm.

The frequency response of proposed dual-side resonators is shown in Figure 10. As can be seen from the frequency response, these resonators create two transmission zeros with more than a 60 dB attenuation level.
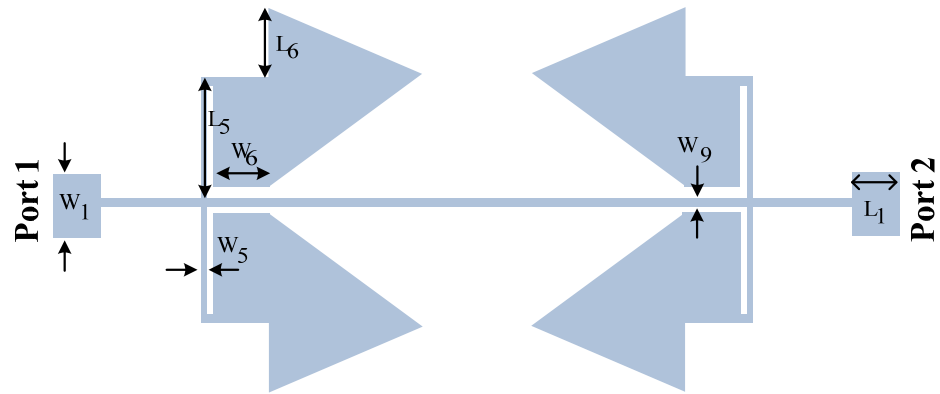
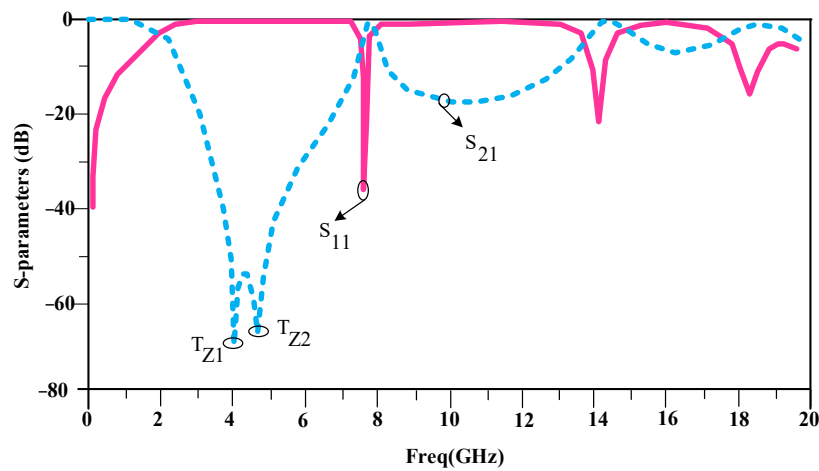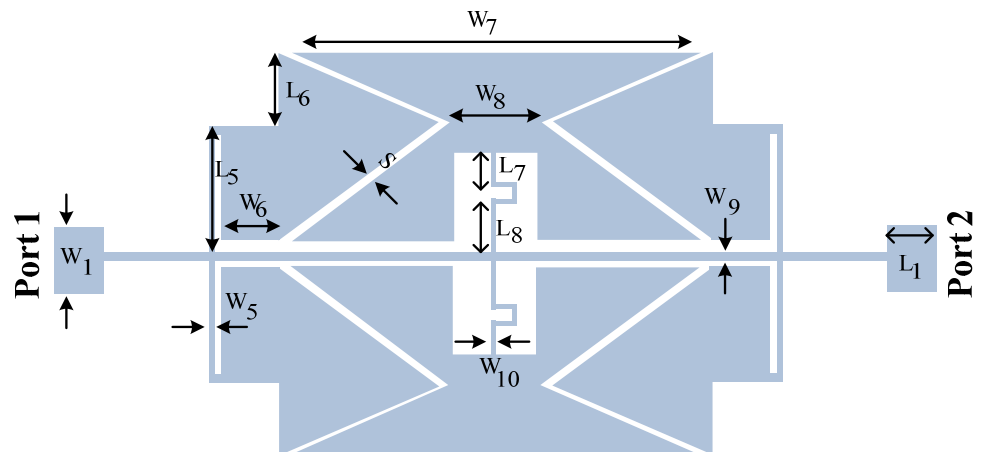**Figure 9.** The structure of the proposed dual-side resonators.

Figure 10. The S-parameters results of the proposed dual-side resonators.

4.2. Proposed Combined Resonator Design

As seen in the previous structures, the obtained frequency responses are not perfect, because these responses do not have a wide stop-band bandwidth, and none of these responses have a proper sharpness in the transition band. Therefore, to improve the frequency response, a combination of these resonators is proposed, as shown in Figure 11. The dimensions of the proposed combined resonator, which are depicted in Figure 11, are listed as follows: L_1 = 1.2 mm, W_1 = 1.56 mm, L_5 = 3 mm, W_5 = 0.1 mm, L_6 = 1.8 mm, W_6 = 1.4 mm, L_7 = 0.8 mm, W_7 = 9.9 mm, L_8 = 0.8 mm, W_8 = 2.2 mm, W_9 = 0.1 mm, W_{10} = 0.2 mm, S = 0.2 mm, L_T = 19.3 mm, W_T = 9.9 mm.

Figure 11. The structure of the proposed combined resonator.

The frequency response of proposed combined resonator is shown in Figure 12. As seen, the proposed combined resonator creates three transmission zeros and provides a wide stop band bandwidth from approximately 1.9 GHz to 8.9 GHz, with an attenuation level of more than 20 dB. The proposed combined resonator has a sharp transition band of about 0.294 GHz from −3 to −20 dB, which provides a 57.8 dB/GHz roll of the rate parameter, which is a desirable result.
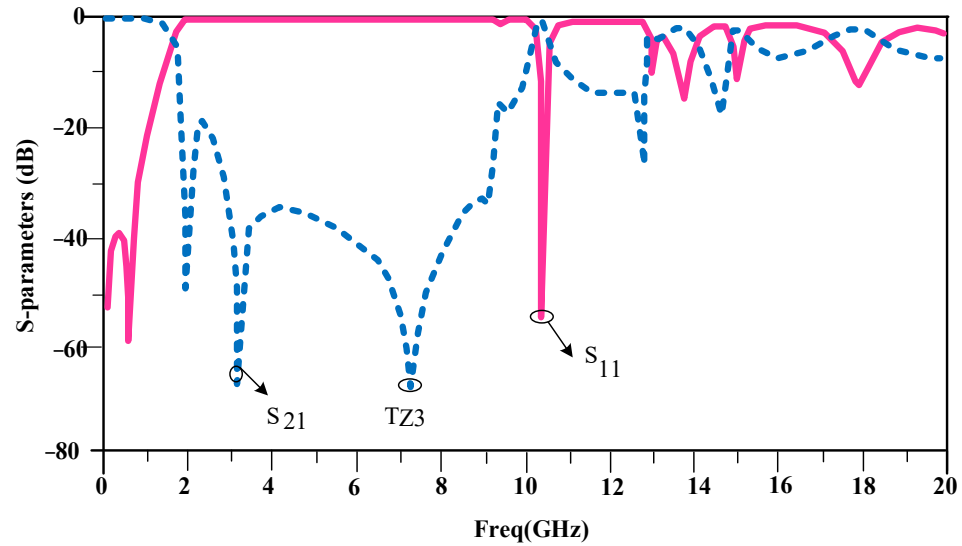

Figure 12. The S-parameter results of the proposed combined resonator.

4.3. Proposed Suppressor Cell Design

The proposed combined resonator described in the previous subsection has a good performance at low frequencies, but in order to obtain attenuation at higher frequencies, suppressor cells should be added to the combined resonator. The structure of the suppressor cells is depicted in Figure 13. The dimensions of the proposed suppressors cells, as depicted in Figure 13, are listed as follows: $L_1 = 1.2$ mm, $W_1 = 1.56$ mm, $L_2 = 6.5$ mm, $W_2 = 0.3$ mm, $L_3 = 9.8$ mm, $W_3 = 0.8$ mm, $L_4 = 4.2$ mm, $W_4 = 1$ mm, $W_9 = 0.1$ mm. The frequency response of the proposed suppressor cells is shown in Figure 14. As seen, the suppressor cells provide suppression at higher frequencies.

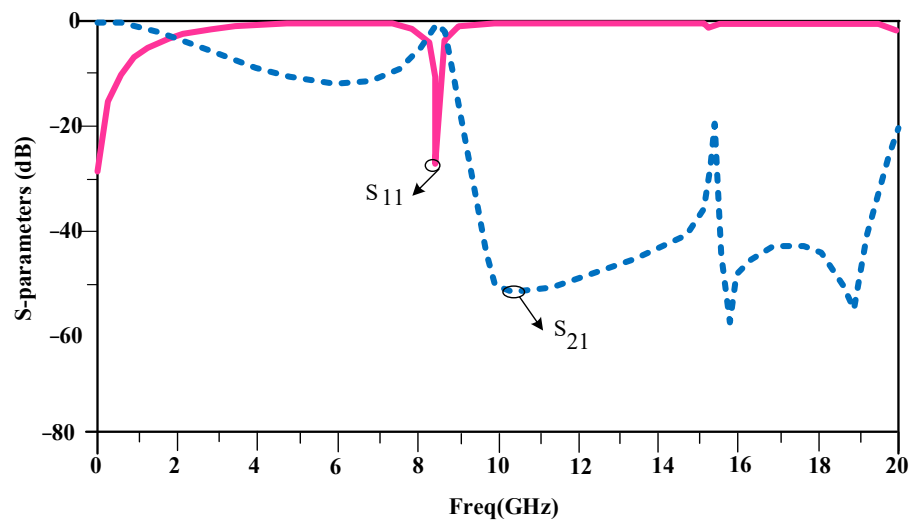**Figure 13.** The structure of the suppressor cells.

Figure 14. The S-parameter results of the suppressor cells.

4.4. Proposed Low-Pass Filter

A schematic of the proposed LPF is depicted in Figure 15. The presented LPF is used in the power divider structure. Therefore, the designed LPF should have a small size. An RT/Duroid 5880 substrate is used to design the LPF; using the aforementioned substrate, the overall size of the LPF is only 19.3 mm × 9.9 mm (0.15 λg × 0.081 λg), and with this small size, the designed LPF may be used in the divider structure.
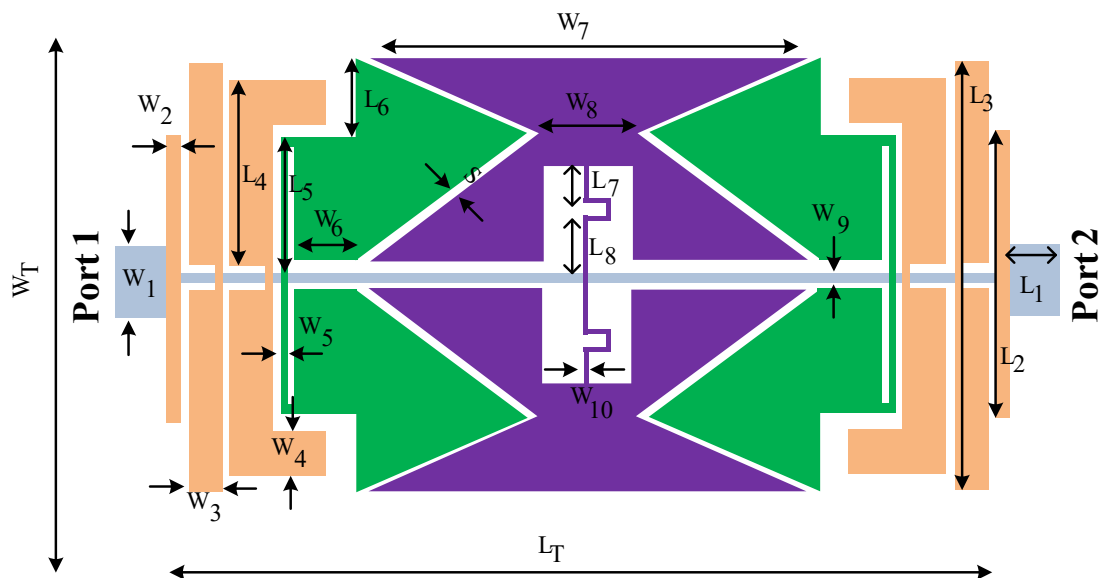
Figure 15. The structure of the proposed low-pass filter.

The proposed LPF consists of designed resonators and suppressed cells. The dimensions of the applied stubs are listed as follows, in which all dimensions are in millimeters: $L_1 = 1.2$, $L_2 = 6.5$, $L_3 = 9.8$, $L_4 = 4.2$, $L_5 = 3$, $L_6 = 1.8$, $L_7 = 0.8$, $L_8 = 0.8$, $W_1 = 1.56$, $W_2 = 0.3$, $W_3 = 0.8$, $W_4 = 1$, $W_5 = 0.1$, $W_6 = 1.4$, $W_7 = 9.9$, $W_8 = 2.2$, $W_9 = 0.1$, $W_{10} = 0.2$, $S = 0.2$, $L_T = 19.3$, $W_T = 9.9$.

The frequency response (S_{11} and S_{21} parameters) of the proposed LPF is depicted in Figure 16. As results shown, the proposed LPF has a 1.8 GHz cut of frequency, and passes signals below this frequency with a very low insertion loss that is close to zero.
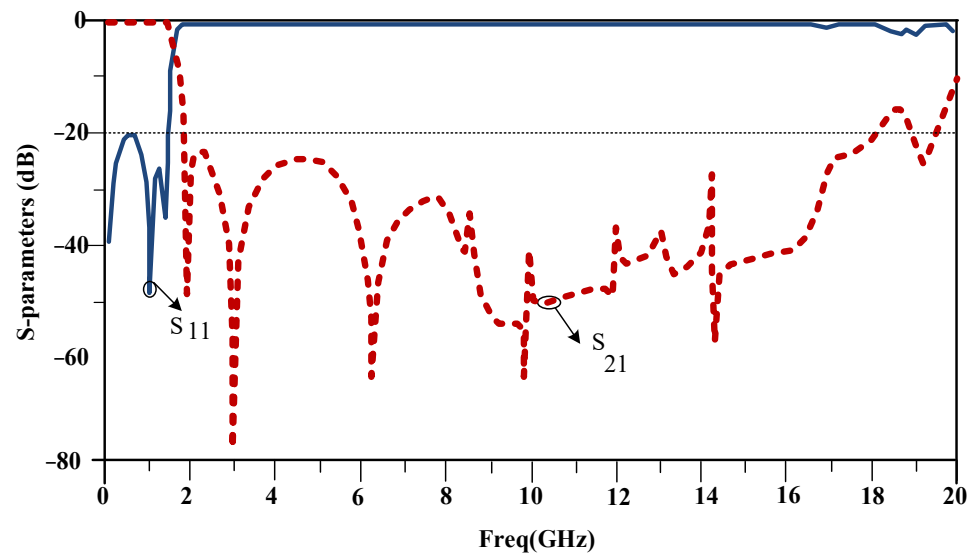
Figure 16. The frequency response of the proposed low-pass filter.

The performance of the proposed LPF is listed and compared with similar related filters in Table 3. The results show the good performance of the proposed LPF. In this table, the roll-off rate (ζ) parameter is defined as in Equation (3):

$$\zeta = \frac{\alpha_{max} - \alpha_{min}}{f_s - f_c} \ (\text{dB/GHz}) \tag{3}$$

where α_{max} and α_{min} are the 40 dB and 3 dB attenuation values, and f_s and f_c are the corresponding frequencies at 40 dB and 3 dB, respectively. In the proposed LPF, at a frequency of 1.8 GHz, the value of parameter S_{21} is equal to -3 dB, and at a frequency of 2 GHz, it is equal to -40 dB. Therefore, according to Equation (3), the obtained roll-off rate (ζ) parameter is about 185 dB/GHz. The related stopband bandwidth (RSB) is defined in Equation (4):

$$\text{RSB} = \frac{\text{stopband} \ (-20 \ \text{dB})}{\text{stopband centre frequency}} \tag{4}$$

Table 3. The performance results of the proposed LPF compared with similar filters.

FOM	AF	NCS	SF	RSB	ζ	Refs.
62,520	1	0.126 λg × 0.055 λg	2.4	1.73	103.9	[10]
11,221	1	0.12 λg × 0.071 λg	1.7	1.52	37	[50]
1159.3	1	0.12 λg × 0.063 λg	1.6	1.66	5.3	[51]
27,142	1	0.12 λg × 0.1 λg	3.5	1.61	57.8	[52]
4723	1	0.101 λg × 0.15 λg	1	1.63	44	[53]
9065	1	0.111 λg × 0.091 λg	1.5	1.65	37	[54]
7095	1	0.14 λg × 0.18 λg	2	1.65	43	[55]
4464	1	0.23 λg × 0.22 λg	2	1.45	62	[56]
49,843	1	0.15 λg × 0.081 λg	2	1.63	185	This work

The proposed LPF has an ultra-wide stopband from 2 GHz to 20 GHz, with attenuation of more than 20 dB. Therefore, the RSB parameter for the designed LPF is equal to 1.63. The suppression factor (SF) parameter is defined in Equation (5). With a 20 dB attenuation level in the stop band, the suppression factor (SF) parameter is equal to 2 in the proposed LPF.

$$\text{SF} = \frac{\text{rejection level in stopband}}{10} \tag{5}$$

The normalized circuit size (NCS) is defined in Equation (6):

$$\text{NCS} = \frac{\text{physical size (length} \times \text{width)}}{\lambda g^2} \tag{6}$$

The proposed LPF has a small size of 19.3 mm × 9.9 mm, which is equal to 0.15 λg × 0.081 λg. The architecture factor (AF) parameter corresponds to the planar or 3D structure, which is equal to 1 for two-dimensional (2D) circuits and equal to 2 for three-dimensional (3D) circuits. For the proposed LPF, the AF is defined as 1. Finally, the figure of merit (FOM) parameter is calculated as written in Equation (7):

$$\text{FOM} = \frac{\zeta \times RSB \times SF}{NCS \times AF} \tag{7}$$

5. The Proposed Wilkinson Divider Design Process

The proposed WPD is obtained by incorporating the designed filters into the conventional WPD structure. The structure of the proposed divider is depicted in Figure 17. In the divider structure, one open-ended stub and two filters are used to suppress unwanted harmonics. The RT/Duroid 5880 substrate is used to simulate the proposed divider.
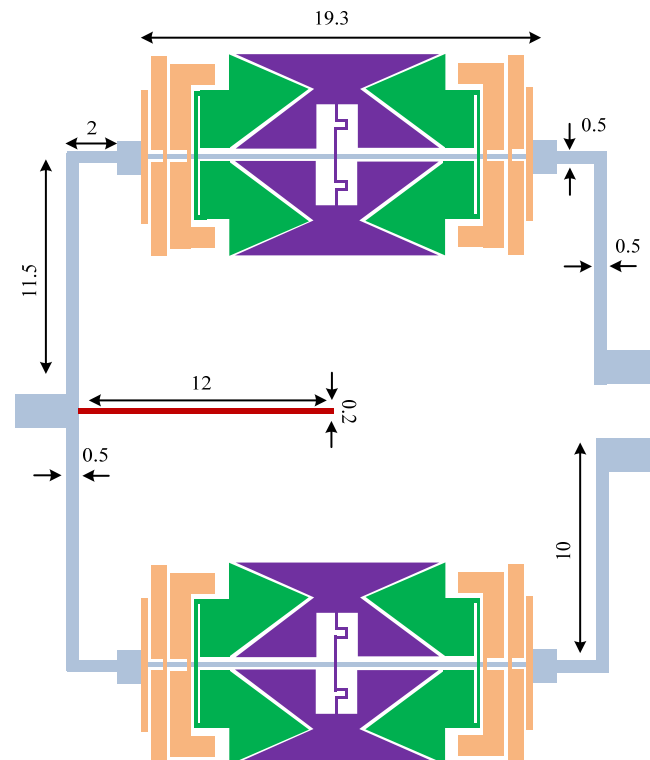

Figure 17. The structure of the proposed Wilkinson power divider.

The frequency response of the proposed Wilkinson power divider is depicted in Figure 18. As the results show, the designed divider has good performance at an operating frequency of 1.5 GHz. The proposed WPD only has a 0.1 dB insertion loss ($S_{12} = -3.1$ dB). Both of the input and output return losses are higher than 30 dB ($S_{11} = -35$ dB, $S_{22} = -30$ dB), and an output ports isolation ($S_{23} = -32$ dB) of more than 32 dB is obtained for the proposed design. Moreover, the proposed divider provides wide rejection band from 2 GHz to 20 GHz, with an attenuation level of more than 20 dB, which suppresses the 2nd–13th unwanted harmonics.
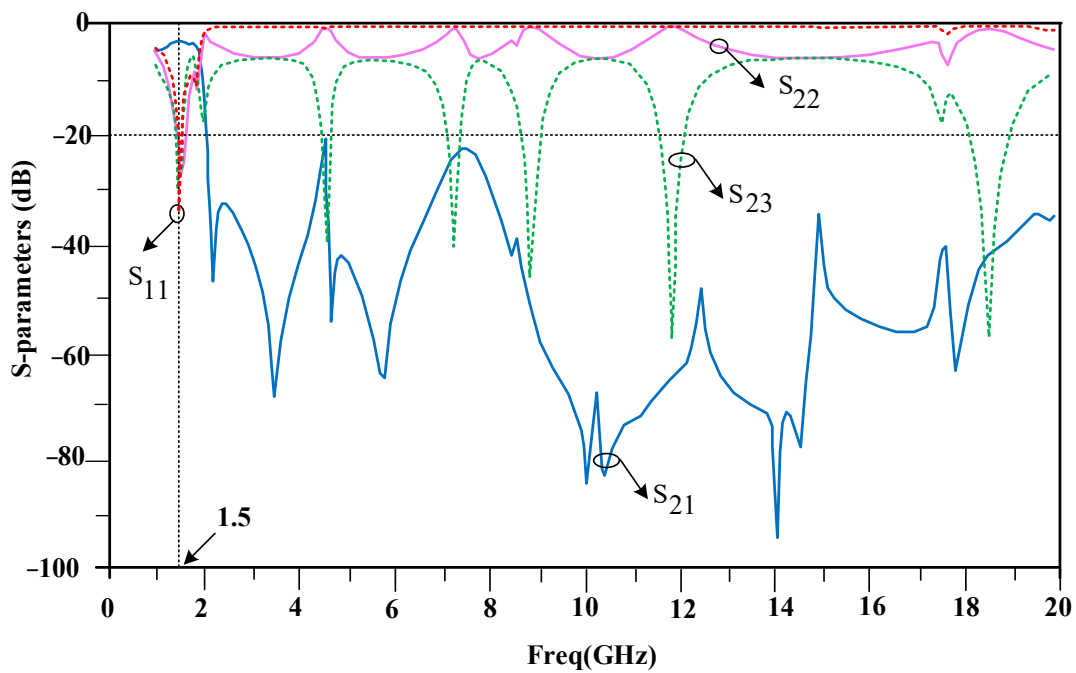
Figure 18. The frequency response of the proposed Wilkinson power divider.

A comparison between the designed divider and some reported works is listed in Table 4. The designed divider shows good performance compared to the other similar works. The proposed divider has good performance at both the operating frequency and at higher frequencies.

Table 4. The performance results of the proposed WPD compared with similar dividers.

Refs.	Frequency	Insertion Loss (IL)	Input Return Loss	Output Return Loss	Output Ports Isolation	Harmonics Suppression
[9]	1 GHz	0.25 dB	40 dB	31 dB	32 dB	2nd to 4th
[11]	2.4 GHz	0.65 dB	22 dB	22 dB	20 dB	2nd and 3rd
[57]	1.8 GHz	0.6 dB	20 dB	20 dB	20 dB	2nd and 3rd
[58]	0.9 GHZ	0.325 dB	36 dB	N.A.	N.A.	3rd
[59]	1 GHz	0.2 dB	30 dB	30 dB	30 dB	3rd to 5th
This work	1.5 GHz	0.1 dB	35 dB	30 dB	32 dB	2nd to 13th

6. Conclusions

This paper demonstrates the successful application of the proposed design algorithm in designing a low-pass filter (LPF) and a power divider. The LPF, designed using the presented algorithm and the proposed artificial neural network (ANN) model, achieves a sharp response within the transmission band, with a sharpness parameter of approximately 185 dB/GHz. It also exhibits excellent performance in the stopband, attaining an attenuation level of more than 20 dB from 2 GHz to 18.2 GHz. The compact size of the LPF (19.3 mm × 9.9 mm, 0.15 λg × 0.081 λg) enables its integration within the divider structure for harmonics suppression. The power divider, consisting of two LPFs in the main branches and an added open stub at port one, effectively operates at 1.5 GHz and successfully suppresses the 2nd to 13th harmonics. The proposed power divider demonstrates superior performance, making it a suitable choice for modern communication systems. Through this paper, we endeavor to highlight the potential of machine learning techniques, particularly neural networks, in advancing microwave circuit design. By harnessing the capabilities of these algorithms, engineers can overcome the limitations of traditional analytical methods, and optimize the performance and reliability of complex microwave circuits.

References

1. Alanazi, A.K.; Alizadeh, S.M.; Nurgalieva, K.S.; Nesic, S.; Grimaldo Guerrero, J.W.; Abo-Dief, H.M.; Eftekhari-Zadeh, E.; Nazemi, E.; Narozhnyy, I.M. Application of neural network and time-domain feature extraction techniques for determining volumetric percentages and the type of two phase flow regimes independent of scale layer thickness. *Appl. Sci.* **2022**, *12*, 1336. [CrossRef]
2. Nazemi, E.; Feghhi, S.; Roshani, G.; Peyvandi, R.G.; Setayeshi, S. Precise void fraction measurement in two-phase flows independent of the flow regime using gamma-ray attenuation. *Nucl. Eng. Technol.* **2016**, *48*, 64–71. [CrossRef]
3. Koziel, S.; Pietrenko-Dabrowska, A. Expedited feature-based quasi-global optimization of multi-band antenna input characteristics with jacobian variability tracking. *IEEE Access* **2020**, *8*, 83907–83915. [CrossRef]
4. Calik, N.; Güneş, F.; Koziel, S.; Pietrenko-Dabrowska, A.; Belen, M.A.; Mahouti, P. Deep-learning-based precise characterization of microwave transistors using fully-automated regression surrogates. *Sci. Rep.* **2023**, *13*, 1445. [CrossRef]
5. Jamshidi, M.; Moztarzadeh, O.; Jamshidi, A.; Abdelgawad, A.; El-Baz, A.S.; Hauer, L. Future of Drug Discovery: The Synergy of Edge Computing, Internet of Medical Things, and Deep Learning. *Future Internet* **2023**, *15*, 142. [CrossRef]
6. Roshani, G.; Nazemi, E.; Roshani, M. Intelligent recognition of gas-oil-water three-phase flow regime and determination of volume fraction using radial basis function. *Flow Meas. Instrum.* **2017**, *54*, 39–45. [CrossRef]
7. Hosseini, S.; Taylan, O.; Abusurrah, M.; Akilan, T.; Nazemi, E.; Eftekhari-Zadeh, E.; Bano, F.; Roshani, G.H. Application of wavelet feature extraction and artificial neural networks for improving the performance of gas–liquid two-phase flow meters used in oil and petrochemical industries. *Polymers* **2021**, *13*, 3647. [CrossRef]
8. Roshani, S.; Azizian, J.; Roshani, S.; Jamshidi, M.; Parandin, F. Design of a miniaturized branch line microstrip coupler with a simple structure using artificial neural network. *Frequenz* **2022**, *76*, 255–263. [CrossRef]
9. Cheng, K.-K.M.; Ip, W.-C. A novel power divider design with enhanced spurious suppression and simple structure. *IEEE Trans. Microw. Theory Tech.* **2010**, *58*, 3903–3908. [CrossRef]
10. Roshani, S.; Yahya, S.I.; Mezaal, Y.S.; Chaudhary, M.A.; Al-Hilali, A.A.; Mojirleilani, A.; Roshani, S. Design of a Compact Quad-Channel Microstrip Diplexer for L and S Band Applications. *Micromachines* **2023**, *14*, 553. [CrossRef]
11. Gu, J.; Sun, X. Miniaturization and harmonic suppression rat-race coupler using C-SCMRC resonators with distributive equivalent circuit. *IEEE Microw. Wirel. Compon. Lett.* **2005**, *15*, 880–882.
12. Koziel, S.; Pietrenko-Dabrowska, A. On nature-inspired design optimization of antenna structures using variable-resolution EM models. *Sci. Rep.* **2023**, *13*, 8373. [CrossRef]
13. Koziel, S.; Pietrenko-Dabrowska, A.; Ullah, U. Low-cost modeling of microwave components by means of two-stage inverse/forward surrogates and domain confinement. *IEEE Trans. Microw. Theory Tech.* **2021**, *69*, 5189–5202. [CrossRef]
14. Koziel, S.; Pietrenko-Dabrowska, A. Constrained multi-objective optimization of compact microwave circuits by design triangulation and pareto front interpolation. *Eur. J. Oper. Res.* **2022**, *299*, 302–312. [CrossRef]
15. Pietrenko-Dabrowska, A.; Koziel, S. Antenna modeling using variable-fidelity EM simulations and constrained co-kriging. *IEEE Access* **2020**, *8*, 91048–91056. [CrossRef]
16. Moztarzadeh, O.; Jamshidi, M.; Sargolzaei, S.; Jamshidi, A.; Baghalipour, N.; Malekzadeh Moghani, M.; Hauer, L. Metaverse and Healthcare: Machine Learning-Enabled Digital Twins of Cancer. *Bioengineering* **2023**, *10*, 455. [CrossRef] [PubMed]
17. Shum, K.M.; Xue, Q.; Chan, C.H. A novel microstrip ring hybrid incorporating a PBG cell. *IEEE Microw. Wirel. Compon. Lett.* **2001**, *11*, 258–260. [CrossRef]
18. Oraizi, H.; Esfahlan, M.S. Miniaturization of Wilkinson power dividers by using defected ground structures. *Prog. Electromagn. Res. Lett.* **2008**, *4*, 113–120. [CrossRef]
19. Woo, D.-J.; Lee, T.-K. Suppression of harmonics in Wilkinson power divider using dual-band rejection by asymmetric DGS. *IEEE Trans. Microw. Theory Tech.* **2005**, *53*, 2139–2144.
20. Yu, X.; Sun, S. A novel wideband filtering power divider with embedding three-line coupled structures. *IEEE Access* **2018**, *6*, 41280–41290. [CrossRef]
21. Roshani, S.; Yahya, S.I.; Roshani, S.; Rostami, M. Design and fabrication of a compact branch-line coupler using resonators with wide harmonics suppression band. *Electronics* **2022**, *11*, 793. [CrossRef]
22. Coromina, J.; Velez, P.; Bonache, J.; Martín, F. Branch line couplers with small size and harmonic suppression based on non-periodic step impedance shunt stub (SISS) loaded lines. *IEEE Access* **2020**, *8*, 67310–67320. [CrossRef]

23. Kumar, M.; Islam, S.N.; Sen, G.; Parui, S.K.; Das, S. Design of compact Wilkinson power divider and branch line coupler using hairpin based line. *AEU-Int. J. Electron. Commun.* **2019**, *110*, 152825. [CrossRef]
24. Luo, M.; Xu, X.; Tang, X.-H.; Zhang, Y.-H. A Compact Balanced-to-Balanced Filtering Gysel Power Divider Using $\lambda_g/2$ Resonators and Short-Stub-Loaded Resonator. *IEEE Microw. Wirel. Compon. Lett.* **2017**, *27*, 645–647. [CrossRef]
25. Li, Q.; Zhang, Y.; Wu, C.-T.M. High-selectivity and miniaturized filtering Wilkinson power dividers integrated with multimode resonators. *IEEE Trans. Compon. Packag. Manuf. Technol.* **2017**, *7*, 1990–1997. [CrossRef]
26. Roshani, S.; Koziel, S.; Roshani, S.; Hashemi Mehr, F.S.; Szczepanski, S. Design and implementation of a dual-band filtering Wilkinson power divider using coupled T-shaped dual-band resonators. *Energies* **2022**, *15*, 1189. [CrossRef]
27. Lotfi, S.; Roshani, S.; Roshani, S. Design of a miniaturized planar microstrip Wilkinson power divider with harmonic cancellation. *Turk. J. Electr. Eng. Comput. Sci.* **2020**, *28*, 3126–3136.
28. Zhang, J.; Cui, B.; Gu, J.-Z.; Sun, X.-W. A harmonic suppressed Wilkinson power divider using complementary split ring resonators (CSRRs). *J. Electromagn. Waves Appl.* **2007**, *21*, 811–819. [CrossRef]
29. Wen, P.; Ma, Z.; Liu, H.; Zhu, S.; Ren, B.; Song, Y.; Wang, X.; Ohira, M. Dual-band filtering power divider using dual-resonance resonators with ultrawide stopband and good isolation. *IEEE Microw. Wirel. Compon. Lett.* **2019**, *29*, 101–103. [CrossRef]
30. Wang, Z.; Jang, J.-S.; Park, C.-W. Tri-band Wilkinson power divider using resonators. In Proceedings of the 2011 IEEE Radio and Wireless Symposium, Phoenix, AZ, USA, 7 March 2011; pp. 287–290.
31. Shao, J.-Y.; Huang, S.-C.; Pang, Y.-H. Wilkinson power divider incorporating quasi-elliptic filters for improved out-of-band rejection. *Electron. Lett.* **2011**, *47*, 1288–1289. [CrossRef]
32. Parandin, F.; Olyaee, S.; Kamarian, R.; Jomour, M. Design and simulation of linear all-optical comparator based on square-lattice photonic crystals. In Proceedings of the Photonics, Kuala Lumpur, Malaysia, 8–10 August 2022; p. 459.
33. Parandin, F.; Moayed, M.; Heidari, F. All-optical diode for terahertz optical power rectification based on two-dimensional photonic crystals. *Microelectron. J.* **2023**, *136*, 105779. [CrossRef]
34. Askarian, A.; Parandin, F. A novel proposal for all optical 1-bit comparator based on 2D linear photonic crystal. *J. Comput. Electron.* **2023**, *22*, 288–295. [CrossRef]
35. Parandin, F.; Sheykhian, A. Design and simulation of a 2×1 All-Optical multiplexer based on photonic crystals. *Opt. Laser Technol.* **2022**, *151*, 108021. [CrossRef]
36. Parandin, F.; Mahtabi, N. Design of an ultra-compact and high-contrast ratio all-optical NOR gate. *Opt. Quantum Electron.* **2021**, *53*, 666. [CrossRef]
37. Parandin, F.; Sheykhian, A.; Bagheri, N. A novel design for an ultracompact optical majority gate based on a ring resonator on photonic crystal substrate. *J. Comput. Electron.* **2023**, *22*, 716–722. [CrossRef]
38. Jamshidi, M.B.; Roshani, S.; Talla, J.; Roshani, S.; Peroutka, Z. Size reduction and performance improvement of a microstrip Wilkinson power divider using a hybrid design technique. *Sci. Rep.* **2021**, *11*, 7773. [CrossRef]
39. Huang, W.; Liu, C.; Yan, L.; Huang, K. A miniaturized dual-band power divider with harmonic suppression for GSM applications. *J. Electromagn. Waves Appl.* **2010**, *24*, 81–91. [CrossRef]
40. Kość, A.; Di Maria, A.; Limbach, M.; Horn, R.; Reigber, A. A 5 way lumped-elements Wilkinson power divider. In Proceedings of the 2013 7th European Conference on Antennas and Propagation (EuCAP), Gothenburg, Sweden, 8–12 April 2013; pp. 357–360.
41. Wu, Y.; Liu, Y. Closed-form design method for unequal lumped-elements Wilkinson power dividers. *Microw. Opt. Technol. Lett.* **2009**, *51*, 1320–1324. [CrossRef]
42. Kawai, T.; Nagano, K.; Enokihara, A. A 920MHz lumped-element Wilkinson power divider utilizing LC-ladder circuits. *IEICE Trans. Electron.* **2018**, *101*, 801–804. [CrossRef]
43. Gao, N.; Wu, G.; Tang, Q. Design of a novel compact dual-band Wilkinson power divider with wide frequency ratio. *IEEE Microw. Wirel. Compon. Lett.* **2013**, *24*, 81–83. [CrossRef]
44. Jamshidi, M.; Farhadi, R.; Jamshidi, M.; Shamsi, Z.; Naseh, S. Using a soft computing method for impedance modelling of li-ion battery current. *Int. J. Adv. Intell. Paradig.* **2020**, *16*, 18–29. [CrossRef]
45. Shafiei, A.; Jamshidi, M.; Khani, F.; Talla, J.; Peroutka, Z.; Gantassi, R.; Baz, M.; Cheikhrouhou, O.; Hamam, H. A Hybrid Technique Based on a Genetic Algorithm for Fuzzy Multiobjective Problems in 5G, Internet of Things, and Mobile Edge Computing. *Math. Probl. Eng.* **2021**, *2021*, 9194578. [CrossRef]
46. Nielsen, M.A. *Neural Networks and Deep Learning*; Determination Press: San Francisco, CA, USA, 2015; Volume 25.
47. Bishop, C. *Neural Networks for Pattern Recognition*; Oxford University Press: New York, NY, USA, 1996.
48. Goodfellow, I.; Bengio, Y.; Courville, A. *Deep Learning*; MIT Press: Cambridge, MA, USA, 2016.
49. Haykin, S. *Neural Networks and Learning Machines, 3/E*; Pearson Education India: Delhi, India, 2009.
50. Ting, S.-W.; Tam, K.-W.; Martins, R. Miniaturized microstrip lowpass filter with wide stopband using double equilateral U-shaped defected ground structure. *IEEE Microw. Wirel. Compon. Lett.* **2006**, *16*, 240–242. [CrossRef]
51. Ma, K.; Yeo, K.S.; Lim, W.M. Ultra-wide rejection band lowpass cell. *Electron. Lett.* **2012**, *48*, 99–100. [CrossRef]
52. Zhang, B.; Li, S.; Huang, J. Compact lowpass filter with wide stopband using coupled rhombic stubs. *Electron. Lett.* **2015**, *51*, 264–266. [CrossRef]
53. Luo, S.; Zhu, L.; Sun, S. Stopband-expanded low-pass filters using microstrip coupled-line hairpin units. *IEEE Microw. Wirel. Compon. Lett.* **2008**, *18*, 506–508. [CrossRef]

54. Mohra, A.S. Microstrip low pass filter with wideband rejection using opened circuit stubs and Z-slots defected ground structures. *Microw. Opt. Technol. Lett.* **2011**, *53*, 811–815. [CrossRef]
55. Mandal, A.; Moyra, T. Compact low-pass filter (LPF) with wide harmonic suppression using interdigital capacitor. *Frequenz* **2023**, *77*, 1–8. [CrossRef]
56. Mandal, A.; Moyra, T. Stub Resonator Based Compact Low-Pass Filter (LPF) with Wide Harmonic Suppression. *Prog. Electromagn. Res. C* **2022**, *122*, 31–40. [CrossRef]
57. Zhang, F.; Li, C. Power divider with microstrip electromagnetic bandgap element for miniaturisation and harmonic rejection. *Electron. Lett.* **2008**, *44*, 422–424. [CrossRef]
58. Karthikeyan, S.; Kshetrimayum, R. Compact, harmonic suppressed power divider using open complementary split-ring resonator. *Microw. Opt. Technol. Lett.* **2011**, *53*, 2897–2899. [CrossRef]
59. He, J.; Feng Chen, Z.; Hai Yang, B.; Ying Xiong, M. Miniaturized microstrip Wilkinson power divider with capacitor loading. *Microw. Opt. Technol. Lett.* **2012**, *54*, 61–63. [CrossRef]